

Observations of Sunspot Oscillations in G band and Ca II H line with Solar Optical Telescope on Hinode

Kaori NAGASHIMA¹, Takashi SEKII^{1,2}, Alexander G. KOSOVICHEV³, Hiromoto SHIBAHASHI⁴, Saku TSUNET², Kiyoshi ICHIMOTO², Yukio KATSUKAWA², Bruce W. LITES⁵, Shin'ichi NAGATA⁶, Toshifumi SHIMIZU⁷, Richard A. SHINE⁸, Yoshinori SUEMATSU², Theodore D. TARBELL⁸, and Alan M. TITLE⁸

¹*Department of Astronomical Science, The Graduate University for Advanced Studies (Sokendai), National Astronomical Observatory of Japan, 2-21-1 Osawa, Mitaka, Tokyo, 181-8588
kaorin@solar.mtk.nao.ac.jp*

²*National Astronomical Observatory of Japan, 2-21-1 Osawa, Mitaka, Tokyo, 181-8588*

³*W.W. Hansen Experimental Physics Laboratory, Stanford University, Stanford, CA 94305, USA*

⁴*Department of Astronomy, School of Science, University of Tokyo, Bunkyo-ku, Tokyo 113-0033*

⁵*High Altitude Observatory, National Center for Atmospheric Research, P.O. Box 3000, Boulder, CO 80307, USA*

⁶*Kwasan and Hida Observatories, Kyoto University, Kurabashira, Kamitakara-cho, Takayama, Gifu, 506-1314*

⁷*Institute of Space and Astronautical Science, Japan Aerospace Exploration Agency, 3-1-1 Yoshinodai, Sagami-hara, Kanagawa 229-8510*

⁸*Lockheed Martin Solar and Astrophysics Laboratory, B/252, 3251 Hanover St., Palo Alto, CA 94304, U.S.A.*

(Received 2007 June 12; accepted 2007 September 3)

Abstract

Exploiting high-resolution observations made by the Solar Optical Telescope onboard Hinode, we investigate the spatial distribution of power spectral density of oscillatory signal in and around active region NOAA 10935. The G-band data show that in the umbra the oscillatory power is suppressed in all frequency ranges. On the other hand, in Ca II H intensity maps oscillations in the umbra, so-called umbral flashes, are clearly seen with the power peaking around 5.5 mHz. The Ca II H power distribution shows the enhanced elements with the spatial scale of the umbral flashes over most of the umbra but there is a region with suppressed power at the center of the umbra. The origin and property of this node-like feature remain unexplained.

Key words: Sun: chromosphere — Sun: oscillations — Sun: sunspots

1. Introduction

Oscillations within sunspots have been studied since Beckers & Tallant (1969) discovered the umbral flashes which are transient brightenings in chromospheric lines in the umbra. In addition to oscillations in intensity in various spectral lines, fluctuations in velocity and magnetic field strength were also observed. So far, three types of oscillations have been observed within sunspots: 3 mHz (five-minute) oscillations in the photospheric umbrae, 5 mHz (and high-frequency) oscillations in the chromospheric umbrae, and running penumbral waves (see review articles by Thomas 1985; Lites 1992; Staude 1999; Bogdan 2000 and references therein). This classification may not be so distinct, as some say that the chromospheric oscillations in umbrae (umbral flashes) and the running penumbral waves might be different manifestations of the same phenomenon (Roupe van der Voort et al. 2003; Tziotziou et al. 2007). Three-minute oscillations in the photosphere of umbrae have also been reported, firstly by Beckers & Schultz (1972) although for their detection a possibility of chromospheric contamination has been pointed out since then (see Lites 1992).

How these oscillations are driven remains unestablished, however. Lites (1992) summarized in his review that

two theoretical pictures of the umbral oscillations in the chromosphere were drawn: one was that umbral oscillations are the resonant response of the atmosphere to forcing by a broad-band power sources below, and the other was that the oscillations are driven by a sub-photospheric resonance to fast-mode waves. More recently, Roupe van der Voort et al. (2003) concluded that the umbral flashes are near-acoustic field-guided upward-propagating shock waves. Centeno et al. (2006) also found evidence for shock waves propagating upward in umbral regions. Umbral oscillations were also observed in higher atmosphere; Shibasaki (2001) reported a radio brightness oscillation of 3-minute period above a sunspot umbra and interpreted it as an upward-traveling acoustic wave. Vecchio et al. (2007) reported that magnetic network elements can also channel low-frequency photospheric oscillations into chromosphere even in the quiet region (Jefferies et al. 2006).

The issue of how the oscillations in sunspots are driven, and how the waves that are associated with these oscillations propagate in magnetized atmosphere is important in probing subsurface structure of sunspots using detailed observations of sunspot oscillations, which was first proposed by Thomas et al. (1982) and now is an actively pursued goal of local helioseismology (see, e.g., Kosovichev et

al. 2000). Using local helioseismological technique, one can extract information about subsurface local structures by measuring travel times for given distances of (primarily) acoustic waves. We need detailed knowledge of how these sunspot waves are generated, and how they interact with magnetic field, in our attempt to reveal how the active regions are generated, evolve, and dissipate by local helioseismology.

Solar Optical Telescope (SOT; Tsuneta et al. 2007) onboard Hinode (Kosugi et al. 2007) reveals many fine structures in sunspots, such as the penumbral flows and the light bridges. In this paper, we report initial SOT observations of sunspot oscillations in Ca II H line and G band with unprecedented high resolution. We observe the lower chromospheric oscillations using the Ca II H line data, while the photospheric oscillations are investigated in the G band. As for helioseismic observation in the quiet region with SOT, see Sekii et al. (2007). In section 2, we briefly describe the SOT observations and the data reduction procedure, and what we found on the umbral oscillations are described in section 3. Discussions mainly on the umbral oscillations are given in section 4.

2. Observations and Data Reduction

A fairly round sunspot close to the disk center (NOAA 10935) was observed with the Solar Optical Telescope (SOT) onboard Hinode over a duration of 4 hr 42 minutes (11:18 - 16:00 UT) on January 8, 2007. Using Broadband Filter Imager (BFI; Tsuneta et al. 2007) of SOT, we obtained series of $218 \text{ arcsec} \times 109 \text{ arcsec}$ filtergrams in Ca II H (3968.5 \AA) and G band (4305 \AA) with a cadence of ~ 1 min. The cadence was slightly irregular, although it hardly affects the Fourier analyses we carry out (see Sekii et al. 2007). To reduce the data amount, 2×2 summing was carried out onboard; hence, the pixel size was ~ 0.1 arcsec. About 10 seconds after taking each G-band image, a Ca II H image was taken. During the period, the correlation tracker (CT; Shimizu et al. 2007) was used to stabilize the images. Since CT only estimates and compensates for the movement in the granules, we need additional tracking to account for the proper motion of the sunspot. We used a two-dimensional cross-correlation technique to compute the displacement. The displacement was then smoothed by polynomial fitting before applied to the series of images. The difference between the original displacements and the smoothed ones were less than 0.7 arcsec, and we consider this value as an estimate of the tracking error. The field of view that we used for our analysis is slightly smaller ($201 \text{ arcsec} \times 101 \text{ arcsec}$) than the original one owing to this sunspot tracking. Figure 1 shows intensity maps in the Ca II H line and in the G band. We studied the intensity oscillations in this field of view.

For dark subtraction, flat fielding, and correcting for bad pixels, we used a calibration program provided by the SOT team. Running difference images were used to remove any possible remnant temporal or spatial trend. Then, in each pixel, the intensity difference was normalized by the mean intensity in the two running frames.

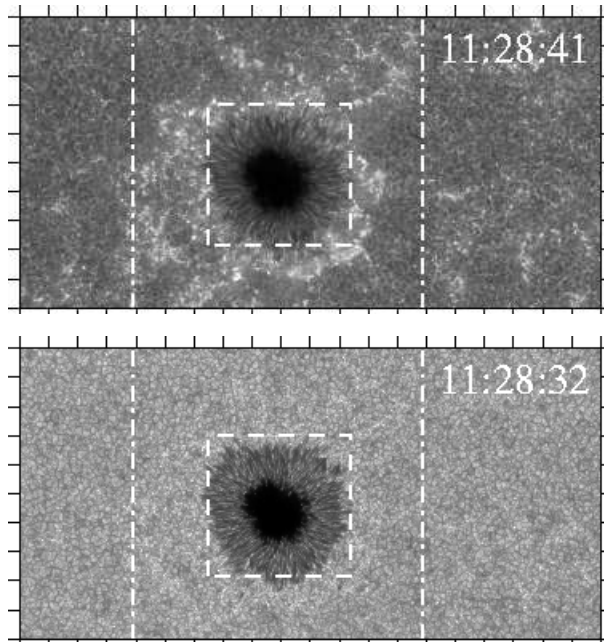


Fig. 1. Sample intensity maps in the Ca II H line (top) and the G band (bottom). We examined the intensity oscillations in this field of view ($201 \text{ arcsec} \times 101 \text{ arcsec}$). The ticks are spaced by 10 arcsec. The central boxes with dashed lines indicate the field of view in figure 2, while the dot-dashed boxes indicate the field of view of the power maps in figures 3 and 6.

This was mainly in attempt to detect oscillations even in the region with very low intensity, i.e., the umbra. It also permits us to observe a smooth transition between umbra and penumbra. We then used Fourier transform of the relative intensity difference time series at each pixel to produce power-spectral-density maps. The Nyquist frequency is 8.3 mHz in our analyses in accordance with the 1-min cadence. Since taking the running difference is equivalent to taking the time derivative on the discrete time grid, we divided the obtained power by squared angular frequency ω^2 . Thus the main remaining effect of taking running difference is the reduced spatial trend.

It should be noted that the power maps measure the intensity variation due to both (magneto)convection and oscillation. These cannot be distinguished by this kind of analysis, except that the convection spectrum is expected to be continuous with a monotonic decrease with frequency.

Another technical point is that because the oscillation spectra are broad-band, normalization by temporally local mean does not affect them very much. We confirmed this by carrying out the analysis without the normalization, where we found no qualitative change, aside from much reduced power in the umbra, which was to be expected.

3. Results

3.1. Umbral Oscillations observed in Ca II H

Figure 2 shows one example of umbral oscillations in our data set. Running difference intensity maps in Ca II H are shown in this figure, except the upper-left panel of the intensity map for reference. Please note that, although here we present the running differences for visual enhancement, power spectra are always corrected for the ω^2 factor. Localized brightening randomly occurs in most of the umbra; in a snapshot of the filtergram, small bright patches are seen. These are “umbral flashes” (e.g., Tziotziou et al. 2007). In the running difference intensity maps, there are some elements with the size of 5 arcsec where a bright region is adjacent to a dark region. Since this means the region with enhanced intensity has just moved from the dark region to the adjacent bright region, we can roughly estimate the propagation speed of the flashes based on separation between these structures; the features moved ~ 4 arcsec in a minute, so the propagation speed is up to 50 km s^{-1} . When we see the running difference movie, these wave-like structure seem to move outward rather than inward. Unlike in the Ca II H data, we cannot find any umbral oscillations in the G-band intensity data.

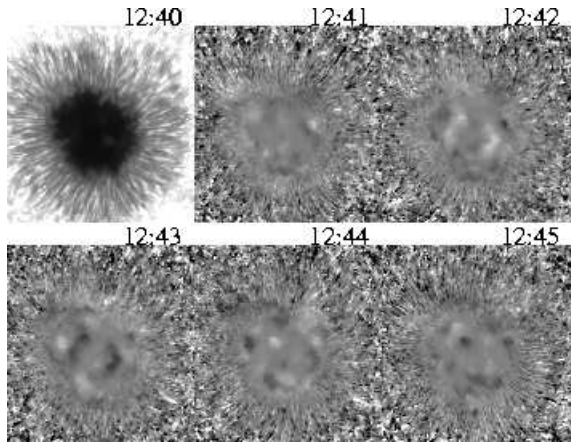


Fig. 2. A Ca II H intensity map (upper-left) and running difference intensity maps (the others) showing umbral oscillations. White marks the region where the intensity increases compared with that in the previous frame. The field of view is a 49-arcsec square. The figure in the upper-right corner of each panel indicates time. An extended version of these figures are available as an mpeg animation in the electronic edition.

3.2. Relative Intensity Power Maps

Since oscillations were seen in the Ca II H running difference intensity movie, we investigated these oscillations in detail by decomposing them into Fourier components. Figures 3 and 4 show a sample Ca II H intensity map and the power maps derived from the Ca II H intensity data. In figure 3, we show the relative intensity power maps averaged over 1 mHz wide frequency ranges, from 1 mHz to 7 mHz with logarithmic greyscaling, while in the figure 4

the power map averaged over the wider frequency range from 0.5 mHz to 7.5 mHz. Figure 5 shows the cross sections of the power maps: we consider circles around the center of the ‘node’ (the center of the dotted circle shown in figure 4) and average the power on each circle to obtain the azimuthally averaged power distribution as a function of the distance from the center of the node. The solid curve indicates the cross section of the averaged power map (figure 4), while the dotted, dashed, and dot-dashed curves show the cross section of the power maps averaged over 0.5–3.5 mHz, 3.5–4.5 mHz, 4.5–7.5 mHz ranges, respectively. Figures 6 and 7 are the G-band counterparts of figures 3 and 4. In figure 6, we omit the 6 mHz and 7 mHz power maps, because they are essentially identical to the 5 mHz power map, except throughout the maps the power was smaller than that in 5-mHz range. We find the following from inspecting these power maps:

1. In the Ca II H power maps, in all the frequency ranges, there is a small area (~ 6 arcsec in diameter) near the center of the umbra where the power was suppressed. This node-like structure is seen more clearly in the power maps averaged over a wider frequency range (figure 4) and in its cross section (figure 5). This type of ‘node’ has not been reported so far, except perhaps the ‘calmest umbral position’ found by Tziotziou et al. (2007) in Doppler power maps (however, for discussion of umbral oscillation patterns, see Uchida & Sakurai (1975) who compared their calculation with Giovanelli’s (1972) observation). Possibly, stable high-resolution observation made by Hinode/SOT was required to find such a tiny node, although it is also possible that only a particular type of sunspots, e.g., round ones with axisymmetric geometry, exhibit such node-like structure; we need to observe various types of sunspots to investigate the possible geometrical effects. We discuss this node in more detail later (section 4.2).

2. Above 4 mHz in the Ca II H power maps, power in the umbra is remarkably large. In the power maps averaged over narrower frequency range (0.05 mHz wide, not shown), the region with high power in the umbra seems to be more patchy. This probably corresponds to the elements of umbral flashes mentioned in the previous subsection. We discuss relationships between this structure and the umbral flashes in section 4.2.

3. In the lower-frequency range (1 mHz), the power is enhanced at the umbra/penumbra boundary in G-band power maps. A similar feature was also reported by Hill et al. (2001); a bright ring around a sunspot was seen in their SOHO/MDI intensity power map in the 0–1 mHz range. This bright ring is discussed in section 4.1. In the higher-frequency ranges, this bright region encircling the umbra is also seen although less striking. The dark regions in the power maps are smaller than the umbra in the intensity map because of the bright ring.

4. In the Ca II H power maps, a bright ring in the penumbra is found in lower frequencies, due to penumbral running waves. Lites (1992) reported that chromospheric oscillatory frequency in the penumbra decreases from 4 mHz at the inner boundary to less than 1.5 mHz at the

outer boundary. In the current data, this is seen as the bright ring decreasing in size as the frequency increases.

5. The region with enhanced power in high-frequency ranges around the active region, so-called “acoustic halo” (Braun et al. 1992; Brown et al. 1992), is not found in our power maps. However, this is not inconsistent with the previous works, because acoustic halos were reported to be in the velocity power maps obtained by Dopplergrams, but not in the intensity power maps (Hindman & Brown 1998).

6. In the regions that are outside the sunspot but are bright in the Ca II H intensity (such as moat region and plage-like features), not only Ca II H power map but also the G-band power map, exhibits remarkable suppression of signal in the higher frequency range, say above 5 mHz. Since these regions are where the magnetic field strength is relatively strong, these features suggest that, outside the sunspot, the power is suppressed as the magnetic field strength increases; this confirms the previous view (e.g., Hindman & Brown 1998; Jain & Haber 2002).

3.3. Power Spectra

To see how the power distributions in the umbra, penumbra, and the quiet region differ from each other, we examined the power spectrum in each region. Figure 8 shows the power spectra of the G-band and the Ca II H intensity oscillations. Each power spectrum is averaged over 39303 pixels (in the umbra), 44000 pixels (in the quiet region), 62000 pixels (in the penumbra), or 21500 pixels (around the boundary between the umbra and penumbra). Here, the umbra and penumbra were defined according to the average Ca II H intensity over the observing period. We defined the quiet region as the region that is outside the sunspot and is not bright in Ca II H, and selected a part of this region so that the area is comparable to those of the umbra and penumbra. The boundary between the umbra and penumbra was defined as the annulus with the inner radius of 11 arcsec and the outer radius of 14 arcsec. The center of the annulus is placed at the center of the node (the center of the circle shown in figure 4).

In all the regions, the G-band intensity power decreases almost monotonically with the frequency, except the broad peak around 4 mHz in the quiet region. This peak corresponds to the global five-minute oscillation. The reason for the lack of power excess in the umbral G-band intensity is not understood. The Ca II H intensity power in the quiet region shows the similar trend, while the power spectrum in the penumbra exhibits monotonic decrease, as is expected from the power maps in figure 3, except the narrow peak at 3 mHz. The Ca II H intensity power spectrum in the umbra has two peaks: one around 3 mHz and the other around 5.5 mHz. In the previous works (e.g., a review by Lites 1992), the dominant period of oscillation in the chromosphere was above 5.5 mHz, and, in contrast to our results, no significant power peaks were found in the 3 mHz range. Comparison with the power spectrum around the boundary between the umbra and penumbra in figure 8 indicates that the 3 mHz peaks in the umbral and penumbral spectra originate in

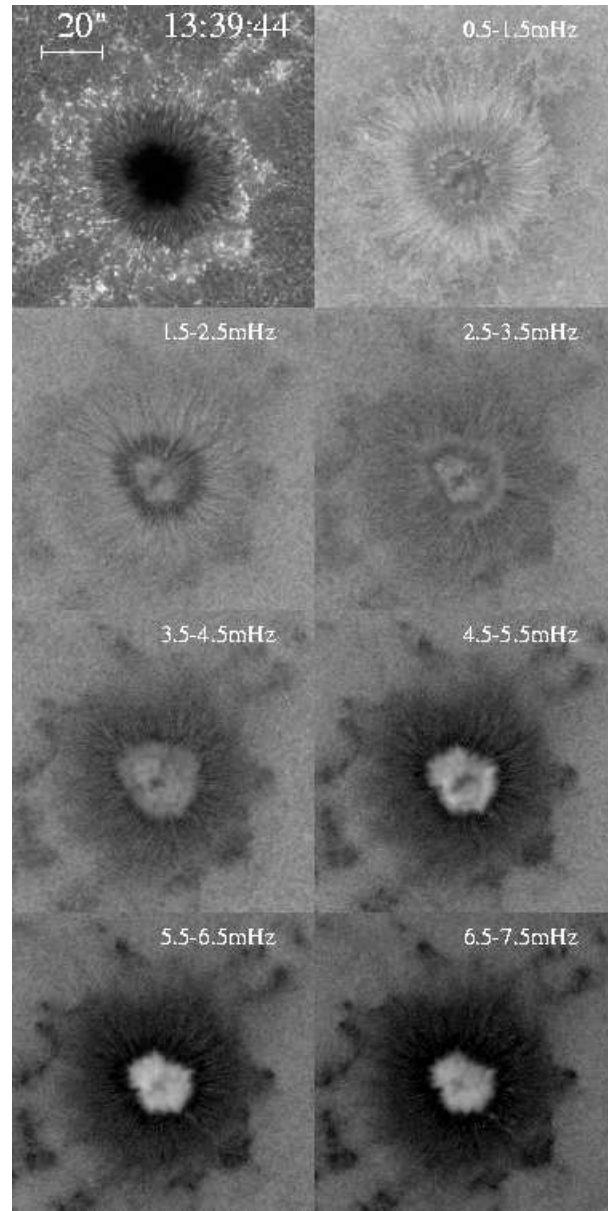


Fig. 3. A Ca II H intensity image (top-left) and the power maps from Ca II H intensity data of active region NOAA 10935. The field of view is 100 arcsec square in all the panels. The power is displayed in logarithmic greyscaling and the same color range is used in figures 3, 4, 6, and 7.

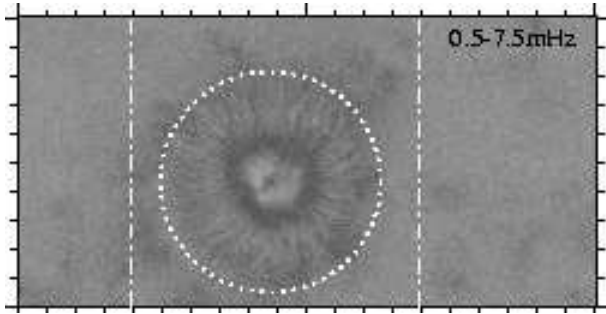


Fig. 4. Ca II H line relative intensity power maps averaged over the frequency range from 0.5 mHz to 7.5 mHz in the full field of view. The dot-dashed lines indicate the field of view in figure 3. The center of the dotted circle is located at the center of gravity of the node-like dark region. The radius of the circle is 38 arcsec, and the cross sections in the circle is shown in figure 5.

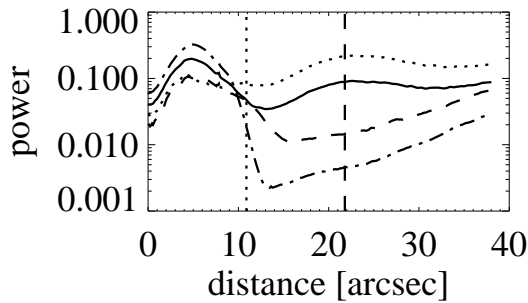


Fig. 5. Cross sections of the Ca II H power map in the sunspot shown in figures 3 and 4. Distance is measured from the center of the node. The solid line indicate the cross section of the power map averaged over the frequency range from 0.5 mHz to 7.5 mHz. The dotted, dashed, and dot-dashed lines indicate the cross section of the power maps averaged over the 0.5–3.5 mHz, 3.5–4.5 mHz, and 4.5–7.5 mHz ranges, respectively. The umbra/penumbra boundary is marked by the dotted vertical line, and the dashed vertical line indicates the penumbra/moat boundary.

the boundary region. The broad peak in the boundary region, between 2 mHz and 5 mHz, is brought about by running penumbral waves.

4. Discussions

4.1. Bright Ring in the Power Maps

As was shown in the G-band power maps in figure 6, there was a bright ring-shaped structure around the penumbra, which appeared in all the frequency ranges, and was most visible in the 1 mHz frequency range. A similar bright ring was reported by Hill et al. (2001). Their power maps derived from SOHO/MDI intensity data showed a bright ring around the sunspot in the 0–1 mHz range. In their case, a strong enhancement of power within a sunspot was also observed in Ca II K intensity in all frequency ranges obtained by TON data only to

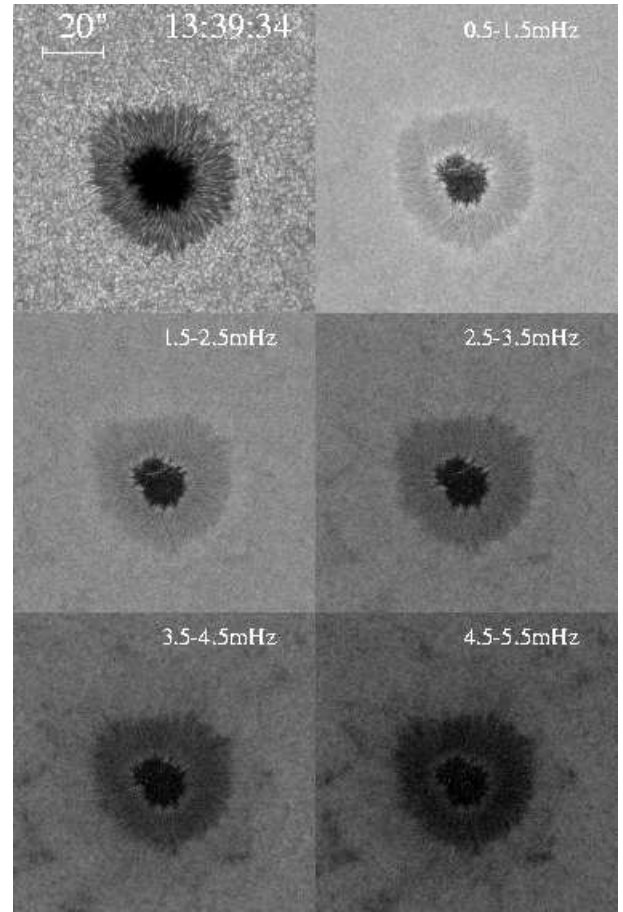


Fig. 6. A G-band intensity image (top-left) and the power maps from G-band intensity data of active region NOAA 10935. The field of view is the same as that in figure 3.

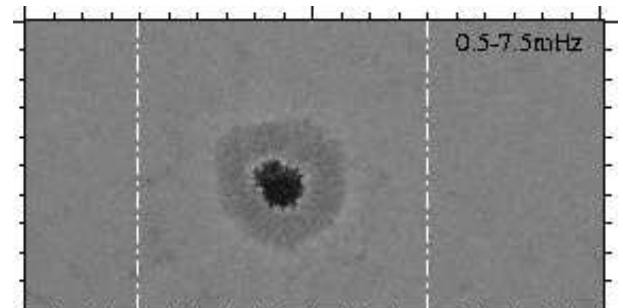


Fig. 7. G-band relative intensity power maps averaged over the frequency range from 0.5 mHz to 7.5 mHz in the full field of view. The dot-dashed lines indicate the field of view in figure 6.

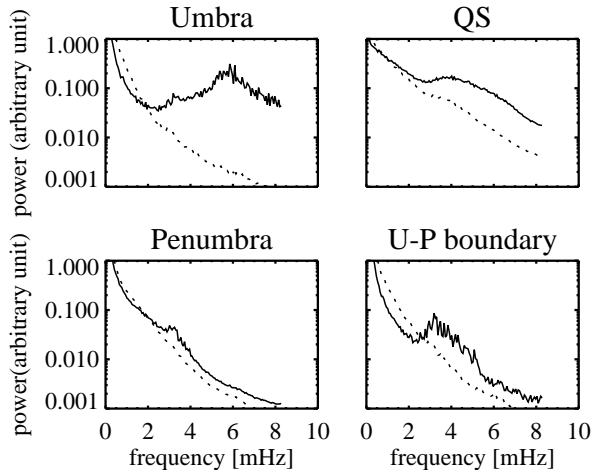


Fig. 8. Power spectra averaged in the umbra (upper left), in the quiet region (upper right), in the penumbra (lower left), and around the boundary between the umbra and the penumbra (lower right). The Ca II H (solid) and the G-band (dotted) intensity power spectra are shown. The ordinate is in an arbitrary unit in logarithmic scale.

be identified as artifacts due to terrestrial seeing. In the case of space-borne observation, seeing never comes into play. There is some possibility that artificial oscillation signals are produced by a poor tracking of the sunspot, since at the sunspot boundary the intensity has large contrast. However, at 0.7 arcsec, the tracking error is smaller than the width of the bright ring around the penumbra (~ 3 arcsec). We therefore conclude the structures are not due to the tracking error. The true nature of this ring is not known, though it seems to be associated with various motions around the umbra/penumbra boundary including penumbral bright filaments breaking into the umbra, and boundary itself moving around by up to ~ 2 arcsec, which is similar to the thickness of the ring, during the observation. These motions themselves may be manifestations of MHD oscillatory phenomena.

4.2. Umbrales Flashes

Umbral flashes are localized transient brightenings in chromospheric umbrae. Since Beckers & Tallant (1969) discovered them in Ca II H and K lines, many observations and theoretical works have been carried out on the subject (e.g., Rouppe van der Voort et al. 2003; Tziotziou et al. 2007). According to them, the period of the umbral flashes is around 3 minutes, and the brightening elements which appear from place to place in the umbrae are 3–5 arcsec wide. In our Hinode/SOT Ca II H data, we confirmed these properties, or at least found the correspondent features: the strong peak around 5.5 mHz in the umbral power spectrum, and the patchy structure of the transient brightenings of about 5 arcsec in the running difference intensity movie. It was also reported that they expand outward in the shape of arcs at the speed of 5–20 km s $^{-1}$ and run into the penumbra. As mentioned in section 3, we find that they seem to move outward at a

speed of up to 50 km s $^{-1}$, as a very rough estimate. For a better estimate, a higher cadence is required.

So far the umbral flashes are interpreted as some kinds of magnetohydrodynamic (MHD) waves (Havnes 1970) and upward-propagating shocks (Rouppe van der Voort et al. 2003; Centeno et al. 2006). Since umbral flashes are known to occur only when the velocity amplitudes exceed a certain threshold (see, e.g., Tziotziou et al. 2007), Rouppe van der Voort et al. (2003) suggested that a large Dopplershift due to upward propagation along the line-of-sight results in a drop of opacity at the line center and causes the brightness enhancements, i.e., the umbral flashes. However, these models do not readily explain the node-like structure we find around the center of the umbra as one then expects the umbral flashes are the most visible in the umbral center. Similar feature to our node-like structure was reported by Tziotziou et al. (2007). In their Doppler velocity maps in Ca II 8542 Å there was a small area around the center of the umbra where the velocity amplitude was lowest. In their paper, intensity fluctuation in the ‘calmest umbral position’ was suggested to be associated with velocity perturbation spreading from the surrounding umbral flashes by means of running waves rather than upward-propagating shocks under conditions different from those in the umbral flashes.

It has to be mentioned that the running umbral waves in the chromosphere reported by Kobanov & Makarchik (2004) may be the same oscillational phenomenon as the umbral flashes. In their study, using H α data instead of Ca II data, they found line-of-sight velocity oscillations in the sunspot umbra, but they did not find the brightenings in H α . Therefore, they concluded that the running umbral waves they found was different from the umbral flashes. However, as they mentioned, brightening in H α does not always accompany the umbral flashes; since the other properties of the running umbral waves are similar to those of the umbral flashes, we cannot exclude the possibility that they are the same phenomenon.

Compared with oscillation signal detected in Dopplergrams, oscillation signal detected in intensity maps is not easily interpretable, because the intensity oscillations are affected not only by the motion of the plasma, but also by how the fluctuation of density, temperature, degree of ionization, and other thermodynamic quantities affect the line formation. Detailed radiative transfer calculation needs to be undertaken. For further study, we need to compare the oscillations in intensity maps with those in Dopplergrams to understand the relationships between the oscillation parameters.

Hinode is a Japanese mission developed and launched by ISAS/JAXA, collaborating with NAOJ as a domestic partner, NASA and STFC (UK) as international partners. Scientific operation of the Hinode mission is conducted by the Hinode science team organized at ISAS/JAXA. This team mainly consists of scientists from institutes in the partner countries. Support for the post-launch operation is provided by JAXA and NAOJ (Japan), STFC (U.K.), NASA, ESA, and NSC (Norway). This work was

carried out at the NAOJ Hinode Science Center, which is supported by the Grant-in-Aid for Creative Scientific Research “The Basic Study of Space Weather Prediction” from MEXT, Japan (Head Investigator: K. Shibata), generous donations from Sun Microsystems, and NAOJ internal funding. K. Nagashima is supported by the Research Fellowship from the Japan Society for the Promotion of Science for Young Scientists.

References

- Beckers, J. M., & Schultz, R. B. 1972, *Sol. Phys.*, 27, 61
Beckers, J. M., & Tallant, P. E. 1969, *Sol. Phys.*, 7, 351
Bogdan, T. J. 2000, *Sol. Phys.*, 192, 373
Braun, D. C., Lindsey, C., Fan, Y., & Jefferies, S. M. 1992, *ApJ*, 392, 739
Brown, T. M., Bogdan, T. J., Lites, B. W., & Thomas, J. H. 1992, *ApJL*, 394, L65
Centeno, R., Collados, M., & Trujillo Bueno, J. 2006, *ApJ*, 640, 1153
Giovannelli, R. G. 1972, *Sol. Phys.*, 27, 71
Havnes, O. 1970, *Sol. Phys.*, 13, 323
Hill, F., Ladenkov, O., Ehgamberdiev, S., & Chou, D.-Y. 2001, ESA SP-464: SOHO 10/GONG 2000 Workshop: Helio- and Asteroseismology at the Dawn of the Millennium, 10, 219
Hindman, B. W., & Brown, T. M. 1998, *ApJ*, 504, 1029
Jain, R., & Haber, D. 2002, *A&A*, 387, 1092
Jefferies, S. M., McIntosh, S. W., Armstrong, J. D., Bogdan, T. J., Cacciani, A., & Fleck, B. 2006, *ApJL*, 648, L151
Kobanov, N. I., & Makarchik, D. V. 2004, *A&A*, 424, 671
Kosovichev, A. G., Duvall, T. L., Jr., & Scherrer, P. H. 2000, *Sol. Phys.*, 192, 159
Kosugi, T., et al. 2007, to be submitted to *Sol. Phys.*
Lites, B. W. 1992, *NATO ASIC Proc. 375: Sunspots. Theory and Observations*, 261
Roupe van der Voort, L. H. M., Rutten, R. J., Sütterlin, P., Sloover, P. J., & Krijger, J. M. 2003, *A&A*, 403, 277
Sekii, T., et al. 2007, submitted to *PASJ*
Shibasaki, K. 2001, *ApJ*, 550, 1113
Shimizu, T., et al. 2007, submitted to *Sol. Phys.*
Staude, J. 1999, *Third Advances in Solar Physics Euroconference: Magnetic Fields and Oscillations*, 184, 113
Thomas, J. H. 1985, *Australian Journal of Physics*, 38, 811
Thomas, J. H., Cram, L. E., & Nye, A. H. 1982, *Nature*, 297, 485
Tsuneta, S., et al. 2007, submitted to *Sol. Phys.*
Tziotziou, K., Tsiropoula, G., Mein, N., & Mein, P. 2007, *A&A*, 463, 1153
Uchida, Y., & Sakurai, T. 1975, *PASJ*, 27, 259
Vecchio, A., Cauzzi, G., Reardon, K. P., Janssen, K., & Rimmele, T. 2007, *A&A*, 461, L1